

# Compton Heated Outflow from CDAFs

Myeong-Gu Park

*Department of Astronomy and Atmospheric Sciences, Kyungpook National University,  
Daegu 702-701, KOREA*

`mgp@knu.ac.kr`

and

Jeremiah P. Ostriker

*Princeton University Observatory, Princeton University, Princeton, NJ 08544;  
Institute of Astronomy, Cambridge, UK*

`jpo@astro.princeton.edu`

## ABSTRACT

Convection-dominated accretion flows (CDAF) are expected to have a shallower density profile and a higher radiation efficiency as compared to advection-dominated accretion flows (ADAF). Both solutions have been developed to account for the observed properties of the low luminosity, high temperature X-ray sources believed to involve accretion onto massive black holes. Self-similar CDAFs also have steeper poloidal density gradients and temperatures close to the virial temperature. All these characteristics make CDAFs more capable of producing polar outflows driven by Compton heating as compared to other classical accretion disks. We investigate the conditions for producing such outflows in CDAFs and look for the mass accretion rate, or, equally, the luminosity of CDAFs for which such outflows will exist. When the electron temperature saturates around  $10^{11}$  K at the inner region, polar outflows are probable for  $8 \times 10^{-7} \lesssim L/L_E \lesssim 4 \times 10^{-5}$ , where  $L_E$  is the Eddington luminosity. Outflows are well collimated with small opening angles. The luminosity range for which outflow solutions exist is narrower for lower electron temperature flows and disappears completely for electron temperature  $\lesssim 6 \times 10^9$  K. When the magnetic field is present, we find that outflows are possible if the magnetic field is less than from 10% to 1% of the equipartition field. We also find that outflows are more likely to be produced when the viscosity parameter  $\alpha$  is small. The tendency for jet-like collimated outflows for these solutions is presumably astrophysically relevant given the high frequency of jets from AGNs.

*Subject headings:* accretion, accretion disks — black hole physics — quasars: general — X-rays: general

## 1. Introduction

Advection-dominated accretion flows (ADAF) nicely complement the classic thin disk accretion flows (Shakura & Sunyaev 1973; Ichimaru 1977; Rees et al. 1982; Narayan & Yi 1994, 1995; Abramowicz et al. 1995), and have been successfully applied to variety of cosmic objects, from galactic X-ray binaries to diffuse X-ray background (see Narayan, Mahadevan, & Quataert 1999 for review). However, analytic studies of ADAFs indicated the convectively unstable nature of ADAFs (Narayan & Yi 1994, 1995a; see Begelman & Meier 1982 for radiation-dominated ADAF), which has subsequently been proved in a series of numerical simulations (Igumenshchev, Chen, & Abramowicz 1996; Igumenshchev & Abramowicz 1999, 2000; Stone, Pringle, & Begelman 1999; Igumenshchev, Abramowicz, & Narayan 2000). Especially, the numerical studies of ADAFs by Igumenshchev & Abramowicz (1999, 2000) show that an ADAF becomes a convection-dominated accretion flow (CDAF) whenever the viscosity parameter  $\alpha \lesssim 0.1$ . Further analyses of self-similar CDAF solutions show their unique properties (Narayan, Igumenshchev & Abramowicz 2000, hereafter NIA; Quataert & Gruzinov 2000, hereafter QG): the density varies as  $\rho \propto R^{-1/2}$  ( $R$  is the radius), much flatter than the usual  $R^{-3/2}$  in an ADAF or in spherical accretion. Correspondingly, the mean radial velocity varies as  $v \propto R^{-3/2}$ , compared to  $R^{-1/2}$  in ADAF or in spherical flow. Energy generated at the inner part of the flow is transported to the outer part by convection. A CDAF has perhaps as much resemblance to the rotating stellar envelope of a massive star as to the usual accretion flow.

The other aspect of the two-dimensional nature of ADAF or CDAF solutions, often neglected, is the interaction between the outgoing radiation produced at smaller radii with the inflowing gas in the outer part of the flow. In optically thick stars this interaction plays a vital role in establishing the equilibrium states. The radiative interaction also plays a very important role in pure spherical accretion flows (Ostriker et al. 1976; Cowie, Ostriker, & Stark 1978; Wandel, Yahil, & Milgrom 1984; Park 1990a, 1990b; Nobili, Turolla, & Zampieri 1991; Zampieri, Miller, & Turolla 1996; Ciotti & Ostriker 1997, 2001). Park & Ostriker (1999, 2001) studied the same radiative interaction in the context of the ADAF solution and found that a polar outflow can be generated through Compton heating of electrons by high-energy photons emitted by the inner, hot part of the flow. The winds generated by the processes in the papers listed above are not momentum driven. Rather, they are caused by overheating of the gas in the slowly moving, low density polar regions. Outflows may also be

generated from ADAF by other hydrodynamic processes (Narayan & Yi 1995; Xu & Chen 1997; Blandford & Begelman 1999).

In this work, we study the conditions for CDAFs to develop radiation driven outflows. We adopt the self-similar CDAF solution as the background flow structure (NIA; QG). The treatment in this paper is two dimensional, adopting the angular profile of NIA and QG, except that the radiation field is simplified and treated as spherically symmetric.

## 2. Flow Properties

### 2.1. Density and Temperature

Multi-dimensional numerical simulations and analytic analyses show that density and temperature profiles of CDAF follow a self-similar form in radius (NIA; QG; Ball, Narayan & Quataert 2001, hereafter BNQ):

$$\rho(r) \propto r^{-1/2} \quad (1)$$

$$T_i(r) \propto r^{-1}, \quad (2)$$

where  $r$  is the radius in units of the Schwarzschild radius,  $R_S \equiv 2GM/c^2 = 3.0 \times 10^5 m$  cm, and  $m$  is the black hole mass in solar units. This shallow radial dependence corresponds to marginal stability to convection. QG further showed that the density should follow a power law in  $\sin \vartheta$  ( $\vartheta$  is the angle from the pole) while the temperature is constant on spherical shells. So we shall assume that the density is given by

$$\rho(r, \vartheta) = \rho_0 r^{-1/2} \sin^2 \vartheta \quad (3)$$

$$= \rho_{out} (r/r_{out})^{-1/2} \sin^2 \vartheta. \quad (4)$$

The flow extends from  $r_{out}$  down to  $r_{in} = 1$ , with the outer radius (analogous to the stellar photosphere) fixed by energy balance considerations.

The electron temperature  $T_e$  in an accretion flow is determined by the balance between various cooling and heating processes. In general, detailed studies of hot accretion flows (Narayan & Yi 1995b; Narayan, Barret, & McClintock 1997; BNQ) show that the electron temperature is equal to the ion temperature for  $T_e \lesssim 10^9$  K, and then, at smaller radii, due to highly efficient relativistic bremsstrahlung and synchrotron emission, it flattens to somewhere between  $10^9$  K to  $10^{11}$  K, depending on the amount of direct viscous heating to electrons. Hence, in this paper, we approximate the electron temperature as

$$T_e(r, \vartheta) = \frac{T_0}{r} \quad \text{for } r > r_1 \quad (5)$$

$$= T_1 \quad \text{for } r \leq r_1, \quad (6)$$

where  $T_0 \approx 10^{12}$  K,  $T_1$  is some constant between  $10^9$  K and  $10^{11}$  K, and  $r_1 \equiv T_0/T_1$ .

From equation (3), we find that the total Thomson optical depth along a given direction  $\vartheta$  is

$$\tau_{es} \simeq \frac{1}{2} \dot{m} r_{out}^{1/2} \sin^2 \vartheta, \quad (7)$$

where  $\dot{m} \equiv \dot{M}/\dot{M}_E = \dot{M}c^2/L_E$  is the dimensionless mass accretion rate. Our analysis, which is to be applied to low accretion rate solutions, will assume that the flow is optically thin to both scattering and redistribution processes.

## 2.2. Radiation Field and Radiation Temperature

The inner part of the accretion flow generally produces higher energy photons, while the outer part produces lower energy photons. Hence the radiation field at a given position is determined by the contribution from inner radiating shells plus the outer shells. Although in each shell, the density, and therefore, the emissivity (i.e. cooling function) is a function of poloidal angle  $\vartheta$ , the energy density is more uniform over angle than is the emissivity. So, we will simplify the calculation of radiative transfer by assuming each radiating shell is homogeneous, using an angle average over the sphere.

Therefore, the radiation energy density at given  $r$ ,  $E_X(r)$ , is given by

$$cE_X(r) = R_s \left[ \frac{1}{4\pi r^2} \int_{r_{in}}^r \Lambda(r') 4\pi r'^2 dr' + \int_r^{r_{out}} \Lambda(r') \frac{r'}{r} \ln \sqrt{\frac{r' + r}{r' - r}} dr' \right], \quad (8)$$

where the first term is the contribution from inner radiating shells and the second term from outer radiating shells (see Appendix A). The emissivity per unit volume is denoted as the cooling function  $\Lambda$ , which will be described in §3.1.

For relativistic un-Comptonized bremsstrahlung, with  $\Lambda \propto \rho^2 T_e$  and CDAF scaling  $\rho \propto r^{-1/2}$  and  $T_e \propto r^{-1}$ , the incremental luminosity  $dL_X(r)/dr = \text{constant}$ , and the luminosity at a given radius  $r$  has the largest contribution from the outermost shell. Nevertheless, equation (8) gives a peak energy density in the inner region (cf. *dashed line* in Fig. 1) and a significant radiation pressure gradient. In addition, when there is strong Comptonization, the contribution from the inner region can be significantly enhanced.

Moreover, the amount of Compton heating is determined by the luminosity times the photon energy, and is largely dominated by the inner hot region. The radiation temperature, defined as  $kT_X(r)$  being the energy-weighted mean photon energy, at a given radius  $r$  is

determined by the equation

$$cT_X(r)E_X(r) = R_S \left[ \frac{1}{4\pi r^2} \int_{r_{in}}^r T_X(r') \Lambda(r') 4\pi r'^2 dr' + \int_r^{r_{out}} T_X(r') \Lambda(r') \frac{r'}{r} \ln \sqrt{\frac{r' + r}{r' - r}} dr' \right]. \quad (9)$$

This quantity is more concentrated than  $E_X(r)$ , especially in the presence of strong Comptonization [see *dotted curve* in Fig. 1 for  $T_X(r)$ ].

In presence of an overheated wind, some region along the pole in CDAF will not be able to accrete matter, while the remaining equatorial region normally accretes (see §3.3). In most of the relevant parameter space, the overheated ‘funnel’ is very narrow, and we assume (with regard to energy generation) that the self-similar CDAF flow is filling the whole space including the polar region, omitting the small correction due to the solid angle  $\Omega_W$  ( $\sim 0.2$  sr) occupied by the outflowing wind/jet.

The resulting profiles of radiation moments and the radiation temperature show the aforementioned characteristics of CDAFs. The luminosity,

$$L(r) = R_S^3 \int_{r_{in}}^r \Lambda(r') 4\pi r'^2 dr', \quad (10)$$

increases at large radius (*solid curve* in Fig. 1), while the radiation temperature is roughly flat or decreasing slowly outward after peaking at some intermediate radius (*dotted curve* in Fig. 1).

### 2.3. Outer Boundary

The mathematical self-similar CDAF has zero mass accretion rate (NIA), and this, of course, corresponds to zero luminosity. However, the accretion flow must lose energy by radiative cooling, and this energy loss is very likely provided by the convective energy transport (NIA, BNQ). We follow BNQ to assume that the total luminosity of ADAF is proportional to the mass accretion rate:

$$L(r_{out}) = \eta_c \epsilon_c \dot{M} c^2, \quad (11)$$

where the convective efficiency  $\epsilon_c$ , determined by numerical simulations to be in the range  $\sim 10^{-2} - 10^{-3}$  and  $\eta_c$  is the fraction of convected energy to be radiated away by electrons. In subsequent examples, we nominally adopt  $\epsilon_c \eta_c = 10^{-2}$  (BNQ). We also tried smaller values of  $\epsilon_c \eta_c$  or a scaling of  $\epsilon_c \eta_c$  with  $\dot{m}$  (cf. §3.3), and the results were qualitatively the same.

We determine the outer boundary for a given mass accretion rate  $\dot{m}$  by finding the radius  $r_{out}$  at which equation (11) is satisfied. This gives a somewhat different relation between the total luminosity and the mass accretion rate from that in BNQ because we have used Comptonized relativistic bremsstrahlung (and synchrotron) while BNQ employ only un-Comptonized non-relativistic bremsstrahlung. However, the general characteristic of the relation is the same: higher mass accretion flows have smaller outer boundary radii. This is due to the special radial profile of density in CDAF solutions. Because of the weak density gradient with radius, most of the luminosity contribution is from the outer part of the flow, which makes CDAF flows quite distinct from other accretion flows including ADAFs. The dimensionless total luminosity,  $L(r_{out})/L_E$ , is directly proportional to the dimensionless mass accretion rate  $\dot{m} \equiv \dot{M}/\dot{M}_E$  by equation (11) while the luminosity accumulated from bremsstrahlung is very roughly proportional to  $\dot{m}^2 r_{out}$  (with a higher power in  $\dot{m}$  if Comptonization is important). Since these two luminosities must be equal, a higher  $\dot{m}$  flow implies a smaller  $r_{out}$  (see *solid lines* in Fig. 2). Therefore lower mass accretion rate CDAF solutions have lower luminosity, yet are more extended, if we treat  $\epsilon_c \eta_c$  as fixed, independent of  $\dot{m}$ .

### 3. Outflow

#### 3.1. Cooling and Heating

The main cooling mechanism we consider in this work is Comptonized bremsstrahlung and Comptonized synchrotron. We first focus on the Comptonized bremsstrahlung. This process is not only the source of electron cooling but also the source of the Compton heating radiation field.

The Comptonized bremsstrahlung cooling rate per unit volume can be reasonably approximated by (Svensson 1982; Stepney & Guilbert 1983)

$$\Lambda_{br} = \sigma_T c \alpha_f m_e c^2 n^2 [F_{ei}(T_e) + F_{ee}(T_e)], \quad (12)$$

where

$$F_{ei} = 4 \left( \frac{2}{\pi^3} \right)^{1/2} \theta_e^{1/2} (1 + 1.781 \theta_e^{1.34}) \quad \text{for } \theta_e < 1 \quad (13)$$

$$= \frac{9}{2\pi} \theta_e [\ln(1.123 \theta_e + 0.48) + 1.5] \quad \text{for } \theta_e > 1$$

$$F_{ee} = \frac{5}{6\pi^{3/2}} (44 - 3\pi^2) \theta_e^{3/2} (1 + 1.1\theta_e + \theta_e^2 - 1.25\theta_e^{5/2}) \quad \text{for } \theta_e < 1 \quad (14)$$

$$= \frac{9}{\pi} \theta_e [\ln(1.123 \theta_e) + 1.2746] \quad \text{for } \theta_e > 1,$$

$\theta_e \equiv kT_e/m_e c^2$ ,  $n$  is the electron (ion) number density,  $\sigma_T$  the Thomson cross section,  $\alpha_f$  the fine structure constant, and  $m_e$  the electron mass. In this work, we assume pure hydrogen gas.

The emitted bremsstrahlung photons are upscattered by inverse Compton scattering. The amplification of photon energy by single scattering is  $A \equiv 1 + 4\theta_e + 16\theta_e^2$ . The probability of single scattering is  $P = 1 - \exp(-\tau_{es})$  (see e.g., Dermer et al. 1991). Therefore the mean amplification factor by Compton scattering would be

$$\eta_0 = 1 - P + PA = 1 + P(A - 1). \quad (15)$$

The fraction  $1 - P$  of photons remain unscattered while the fraction  $P$  of photons are upscattered to  $A$  times their initial energy. This prescription is valid only for a single scattering Comptonization. Since most CDAF flow considered here has  $\tau_{es} < 1$ , we use this amplification factor for Comptonized bremsstrahlung. Although Dermer et al. (1991) provides a handy formula for  $\eta$ , applicable to diverse regimes, it can give incorrect values for  $A \gg 1$  and  $\tau_{es} \lesssim 1$ , the main parameter regime of CDAF. Although  $\tau_{es}$  is a hard-to-define quantity in a complex flow, we simply adopt  $\tau_{es} = n_e \sigma_T r$  in this work for the purpose of estimating the Comptonization.

When  $PA \gg 1$ , Comptonization becomes saturated, and all photons that are not absorbed are upscattered to  $3T_e$ , that is  $\eta \rightarrow \eta_{sat} = 3\theta_e/x$  where  $x \equiv h\nu/m_e c^2$  (Dermer et al. 1991). Then the fully saturated Comptonized bremsstrahlung emission is

$$\Lambda_{Cbr}^{sat} = \int_{x_{abs}}^{3\theta_e} \eta_{sat} \epsilon_{br}(x) dx + \int_{3\theta_e}^{\infty} \epsilon_{br}(x) dx \quad (16)$$

$$= \Lambda_{br} \left[ \int_3^{\infty} e^{-t} dt + \int_{x_{abs}/\theta_e}^3 3t^{-1} e^{-t} dt \right] \quad (17)$$

where  $\epsilon_{br}(x)$  is the bremsstrahlung spectrum

$$\epsilon_{br}(x) = \Lambda_{br} \exp\left(-\frac{x}{\theta_e}\right) dx \quad (18)$$

and  $x_{abs}$  is the absorption frequency  $\nu_{abs}$  in unit of  $m_e c^2/h$ . Since  $\Lambda_{br}$  is smaller by the factor  $\exp(x_{abs}/\theta_e)$  in presence of absorption, we take the maximum amplification factor for bremsstrahlung as

$$\eta_{br}^{sat} = e^{x_{abs}/\theta_e} \times \left\{ e^{-3} + 3 \left[ E_1\left(\frac{x_{abs}}{\theta_e}\right) - E_1(3) \right] \right\}, \quad (19)$$

where  $E_n \equiv \int_1^{\infty} t^{-n} \exp(-xt) dt$  is the exponential integral. The final Comptonized bremsstrahlung emission is then

$$\Lambda_{Cbr} = \min(\eta_0, \eta_{br}^{sat}) \Lambda_{br}. \quad (20)$$

The energy-weighted mean photon energy for unsaturated Comptonized bremsstrahlung is (see e.g. PO2)

$$\frac{4kT_X}{m_e c^2} = \frac{\int_0^\infty \eta_{br}^2 x \epsilon_{br}(x) dx}{\int_0^\infty \eta_{br} \epsilon_{br}(x) dx} = \eta_{br} \theta_e, \quad (21)$$

and that for saturated Comptonized bremsstrahlung is simply

$$T_X = T_e, \quad (22)$$

since the spectrum approaches Wien spectrum which has  $T_X = T_e$ . Therefore, the radiation temperature of locally radiated bremsstrahlung emission is

$$T_X^{Cbr} = \frac{1}{4} T_e \min(\eta_{br}, 4). \quad (23)$$

The frequency  $\nu_{abs}$  is chosen to be the frequency at which the free-free absorption optical depth is equal to 1,

$$r a_{ff}(\nu_{abs}) = 1, \quad (24)$$

where  $a_{ff}$  is the absorption coefficient given by Dermer et al. (1991)

$$a_{ff}(x) = \sqrt{8\pi} \frac{\alpha_f^2 \sigma_T r_e^3}{x^2 \theta_e^{3/2} [1 + (8/\pi)^{1/2} \theta_e^{3/2}]} n_i^2 \bar{g} \quad (25)$$

with

$$\begin{aligned} \bar{g} = & (1 + 2\theta_e + 2\theta_e^2) \ln \left[ \frac{4\eta_E(1 + 3.42\theta_e)\theta_e}{x} \right] \\ & + \left( \frac{3\sqrt{2}}{5} + 2\theta_e \right) \theta_e \ln \left[ \frac{4\eta_E(11.2 + 10.4\theta_e^2)\theta_e}{x} \right], \end{aligned} \quad (26)$$

$\alpha_f$  is the fine structure constant, and  $r_e = e^2/m_e c^2$  the electron radius (Svensson 1984). This expression is valid for  $x \ll \theta_e$  and we used  $(\pi/2)^{1/2} \theta_e^{1/2} [1 + (8/\pi)^{1/2} \theta_e^{3/2}]$  to approximate  $\exp(1/\theta_e) K_2(1/\theta_e)$ .

Flow at a given position is heated (or cooled) by the inverse Comptonization off electrons. We use the heating rate (Levich & Sunyaev 1971)

$$\Gamma_C = 4\sigma_T c [\theta_X(r) - \theta_e(r)] E_X(r) n_e(r, \vartheta), \quad (27)$$

where  $E_X(r)$  is the radiation energy density from equation (8) and  $\theta_X \equiv kT_X/m_e c^2$  the radiation temperature from equation (9).



### 3.2. Equilibrium Temperature and Overheating

In original CDAF, the temperature of the gas is determined by the balance between the viscous heating plus the convective energy transport versus the radiative cooling. However, if the radiative heating is dominant in some region of the flow (the condition under which this assumption is valid is discussed in §3.4.), the temperature in that region will change to reach a new equilibrium. The new equilibrium temperature of the flow will be determined by the balance between radiative heating and radiative cooling.

In CDAF considered in this work, Compton heating versus Comptonized bremsstrahlung cooling are the main radiative processes. The thermal equilibrium temperature  $T_{eq}$ , then, satisfies

$$\Gamma_C(T_{eq}) = \Lambda_{Cbr}(T_{eq}) \quad (28)$$

at given position  $(r, \vartheta)$ . From equations (20) and (27),  $\theta_{eq} \equiv kT_{eq}/m_e c^2$  is determined by

$$4cE_X(r)[\theta_X(r) - \theta_{eq}] = \alpha_f m_e c^3 n_e(r, \vartheta) \eta_{Cbr}(n_e, r, \theta_{eq}) [F_{ei}(\theta_{eq}) + F_{ee}(\theta_{eq})]. \quad (29)$$

Since the number density  $n_e(r, \vartheta)$  decrease as  $\vartheta \rightarrow 0$  (toward the pole), the derived electron temperature increases toward the pole as long as  $\theta_X > \theta_e$ .

For smaller enough  $\vartheta$ , the thermal equilibrium temperature can be higher than the virial temperature,

$$T_{eq}(r, \vartheta) > T_{vir}(r). \quad (30)$$

The virial temperature is defined as  $(5/2)kT_{vir} = m_p GM/r$ , where  $m_p$  is the proton mass. Once electrons are heated above the virial temperature, and therefore above the ion temperature, electrons are likely (via collisions and instabilities) to heat ions to above the virial temperature, thereby, creating winds, especially because the dynamical time of CDAF is much longer than the free-fall flow. Therefore, we adopt equation (30) as the condition for overheating and producing a wind.

What equation (30) means is that some region of CDAF will be radiatively heated from the background temperature  $T_e$  to  $T_{eq}$  to achieve the thermal equilibrium. However, as the temperature of the flow approaches  $T_{eq}$ , it will become unbound when the condition (30) is met, and thereby producing the outflow.

There is also a trivial, yet additional constraint for overheating: the radiation temperature must be higher than the virial temperature

$$T_X(r) > T_{vir}(r), \quad (31)$$

otherwise the radiation field will cool the flow.

### 3.3. Outflow

Outflows will extend from the polar axis to the angle  $\vartheta_c$  at which the equilibrium temperature is equal to the virial temperature,

$$T_{eq}(r, \vartheta_c) = T_{vir}(r). \quad (32)$$

Regions with  $\vartheta < \vartheta_c$  are overheated to above the virial temperature. Hence, the shape of the outflow is determined by the angle  $\vartheta_c(r)$  as a function of  $r$ .

One example of the outflow is shown in Figure 3 for the mass accretion rate of  $\dot{m} = 10^{-3}$ , the electron temperature of inner region  $T_1 = 10^{11}$  K. The *solid curve* shows  $\vartheta_c(r)$ , and the outer *dotted circle* is the outer boundary of the flow. The outflow starts at  $r \simeq 40$  and the opening angle  $\vartheta_c$  reaches maximum of  $17^\circ$  around  $r \simeq 700$  and ends with  $8.3^\circ$  at the outer boundary. Figure 4 shows the same for  $\dot{m} = 2.0 \times 10^{-3}$  and  $T_1 = 3.0 \times 10^{10}$  K with  $\vartheta_c = 6.6^\circ$  at the boundary. The inner isothermal region and the immediate surroundings have  $T_X < T_{vir}$ , and the overheating does not occur. However, at larger radius Compton heating is strong enough to overheat the polar region of the gas and produce outflow. The fraction of the sphere covered by the outflowing gas is  $2\pi\vartheta^2/4\pi \sim 0.01$  for  $\vartheta = 8.3^\circ$ .

We have considered combinations of  $\dot{m}$  and  $T_1$ . Outflow solutions exist within a limited range of these parameters. Too high  $\dot{m}$  makes the outer boundary so small that the whole region is isothermal, i.e.,  $T_X = T_e$ , and the flow is not heated. The outer boundary is smaller for higher  $\dot{m}$  because radiative luminosity is proportional to  $\dot{m}^2$  while CDAF flows have a fixed (assumed) radiation efficiency, which makes the total luminosity roughly proportional to  $\dot{m}$ . The only way to reconcile this is  $r_{out}$  being smaller for higher  $\dot{m}$  (BNQ). In a too low  $\dot{m}$  flow, Comptonization is not strong enough to keep the radiation temperature high. Lower energy photons from larger radii dilute the radiation field and flows are not heated. In Figure 5, we show region of space in  $(\dot{m}, T_1)$  where outflow solutions are successfully produced. *Circles* denote  $(\dot{m}, T_1)$  for which outflows are found. The size of circle represents the opening angle of the outflow at the outer boundary, the majority being  $\lesssim 10^\circ$ . *Crosses* denote  $(\dot{m}, T_1)$  values for which outflows do not exist.

As expected, flows with high electron temperature are more likely to develop outflows. Outflows are not expected for  $T_1 < m_e c^2/k \simeq 6 \times 10^9$  K: Comptonization is less efficient when  $kT_e/m_e c^2 < 1$ . Since the adopted radiation efficiency is  $\epsilon_c \eta_c \simeq 10^{-2}$ , we expect CDAFs with outflows to exist in the luminosity range  $8 \times 10^{-7} \lesssim L/L_E \lesssim 4 \times 10^{-5}$  for  $T_1 = 10^{11}$  K and  $4 \times 10^{-5} \lesssim L/L_E \lesssim 10^{-4}$  for  $T_1 = 10^{10}$  K. These results do not depend on the mass of the black holes.

So far, we have assumed that the total radiation efficiency  $\epsilon_c \eta_c$  is constant. In fact,

current theoretical understanding of the CDAF solution is not yet secure on this point. We now relax that assumption and study an alternative case when  $\epsilon_c \eta_c$  is assumed to be proportional to  $\dot{m}$ . We adopt simply  $\epsilon_c \eta_c = 10^{-2}(\dot{m}/10^{-2})$  so as to make  $\epsilon_c \eta_c = 10^{-2}$  for  $\dot{m} = 10^{-2}$ . Now for small  $\dot{m}$  the total luminosity determined from equation (11) and the total bremsstrahlung emission from equation (10) are both proportional to  $\dot{m}^2$ , and the outer boundary is now at a roughly constant radius (see *dotted lines* in Fig. 2). At high  $\dot{m}$ , Comptonization adds additional power of  $\dot{m}$  to the total emission, and  $r_{out}$  depends on  $\dot{m}$  (see *dotted lines* in Fig. 2). The outflow solutions for this choice of radiation efficiency are shown in Figure 6. Qualitatively, they are not much different from the solutions with constant  $\epsilon_c \eta_c$ . Nonetheless, the flow is much less extended due to lower radiation efficiency for lower  $\dot{m}$  and the shape of the outflow funnel in this case is almost straight. The whole flow structure is quite self-similar except for the magnitude of the opening angle. Most of the solutions still have the opening angle at the outer boundary  $\lesssim 20^\circ$ .

### 3.4. Convection, Heating, and Cooling Timescales

In the original self-similar CDAF, the viscous heating is balanced by the convective energy transport. However, radiative heating can be dominant in some region of the flow. The importance of each heating and cooling process is measured by the corresponding timescale. The radiative heating timescale is given by the ratio between the internal energy of the electron,  $\epsilon_e$ , and the Compton heating rate,

$$t_H \equiv \frac{\epsilon_e}{\Gamma_C}. \quad (33)$$

The radiative cooling timescale is similarly given by

$$t_C \equiv \frac{\epsilon_e}{\Lambda_{Cbr}}. \quad (34)$$

The timescale for convective energy transport at a certain two-dimensional position is not trivial to evaluate because the two-dimensional velocity profile including the convective motion is needed. Although two-dimensional numerical simulations (Stone, Pringle, & Begelman 1999; Igumenshchev, Abramowicz, & Narayan 2000; Igumenshchev & Abramowicz 2000) suggest very limited flow motion near the pole as in self-similar two-dimensional ADAF (Narayan & Yi 1995), the two-dimensional flow motion has yet to be expressed in simple analytic form. Here, we adopt the height-averaged convective energy flux given by NIA,

$$F_c = -\alpha_c \frac{c_s^2}{\Omega_K} \rho T \frac{ds}{dr}, \quad (35)$$

where  $\alpha_c$  is the convection coefficient analogous to the usual Shakura & Sunyaev  $\alpha$ ,  $c_s$  the isothermal sound speed,  $\Omega_K$  the Keplerian angular velocity, and  $s$  the entropy of the flow. In a self-similar solution that is marginally stable to convection,  $\alpha_c = 3\alpha$  is expected when  $\alpha \lesssim 0.05$  (NIA). The cooling rate per volume due to this convective energy flux is then

$$Q_{cv} \equiv \frac{F_c}{r}. \quad (36)$$

Corresponding timescale  $t_{cv}$  is now

$$t_{cv} = \frac{\varepsilon_i}{Q_{cv}}. \quad (37)$$

Since the actual convective motion near the pole is generally much smaller than the average convective motion near the disk midplane as is assumed in equation (35), the actual timescale for the convective cooling could be much longer than  $t_{cv}$  evaluated by equation (37).

For given dimensionless mass accretion rate  $\dot{m}$  and the inner electron temperature  $T_1$ , small  $\alpha$  (of Shakura-Sunyaev), or equally small  $\alpha_c$ , means slower radial motion, and therefore, slower convective motion. So we searched for the critical value of  $\alpha$  below which  $t_{cv} > t_H$  is satisfied within the overheated region. For higher electron temperature of  $T_1 = 10^{11}$  K. the value of the critical  $\alpha$  ranges from  $2.0 \times 10^{-3}$  for  $\dot{m} = 2 \times 10^{-3}$  to  $1.2 \times 10^{-5}$  for  $\dot{m} = 8 \times 10^{-5}$ , all at a constant radiation efficiency of  $10^{-2}$ . For lower electron temperature of  $T_1 = 3 \times 10^{10}$  K. the value of the critical  $\alpha$  ranges from  $2.7 \times 10^{-2}$  for  $\dot{m} = 8 \times 10^{-3}$  to  $3.0 \times 10^{-4}$  for  $\dot{m} = 8 \times 10^{-4}$ . For even lower electron temperature of  $T_1 = 10^{10}$  K at which overheated region is very limited in radius, the value of the critical  $\alpha$  ranges from  $1.6 \times 10^{-2}$  for  $\dot{m} = 10^{-2}$  to  $2.8 \times 10^{-3}$  for  $\dot{m} = 4 \times 10^{-3}$ . Expected values of  $\alpha$  for which CDAF exists are in the range  $\alpha < 0.05$  (NIA). We, therefore, conclude that the Compton heated outflow is expected to be produced in CDAF if the viscosity parameter  $\alpha$  is small enough, exact value being dependent on the mass accretion rate. However, as already mentioned, the real convective motion near the pole is expected to be much smaller than the average convective motion in the disk, the Compton heated outflow near the pole may develop even for much larger value of  $\alpha$ .

Another timescales we want to check are  $t_H$  versus  $t_C$  at the temperature of the background flow  $T_e(r, \vartheta)$  given by equation (5). Only when radiative heating is greater than cooling, i.e.,  $t_H|_{T_e} < t_C|_{T_e}$ , the flow is heated from  $T_e$  to overheated temperature  $T_{eq}$  of equation (28). The ratio  $(t_H/t_C)_{T_e}$  can be expressed as

$$\frac{t_C}{t_H} = \frac{\Gamma_C(T_e)}{\Lambda_{Cbr}(T_e)} = \frac{\Gamma_C(T_{eq})}{\Lambda_{Cbr}(T_{eq})} \frac{\Gamma_C(T_e)}{\Gamma_C(T_{eq})} \frac{\Lambda_{Cbr}(T_{eq})}{\Lambda_{Cbr}(T_e)} = \frac{\Gamma_C(T_e)}{\Gamma_C(T_{eq})} \frac{\Lambda_{Cbr}(T_{eq})}{\Lambda_{Cbr}(T_e)}, \quad (38)$$

which is always less than 1 as long as  $T_{eq} > T_e$  because  $\Gamma_C(T_e)$  is a monotonically decreasing function of  $T_e$  and  $\Lambda_{Cbr}(T_e)$  a monotonically increasing function of  $T_e$ . The ratio  $\Gamma_C(T_{eq})/\Lambda_{Cbr}(T_{eq}) = 1$  by the definition of  $T_{eq}$  in equation (28).

### 3.5. Synchrotron Emission

The synchrotron emission of hot electrons can produce copious soft photons some of which are subsequently Compton upscattered. This will lead to an increase in the total cooling rate as well as a decrease in the radiation temperature of the emitted radiation. Increased cooling rate will reduce the outer boundary of the CDAF whereas decreased radiation temperature will reduce the Compton heating, or even cool the flow if the radiation temperature falls below the electron temperature.

So we recalculated the condition for overheating in presence of magnetic field for the flow parameters considered in Fig. 5. The treatment of Comptonized synchrotron is described in Appendix B. We fix the black hole mass to be  $10^8 M_\odot$ . We find that the synchrotron emission can significantly affect the high temperature flow whereas the low temperature flow is less affected. The overheating and subsequent production of the outflow is still possible for flow with  $T_1 = 10^{10}$  K as long as the magnetic field is less than 10% of the equipartition (the gas pressure being equal to the magnetic pressure) field. The outer boundary of the flow and the opening angle of the outflow are hardly changed if this condition is met. For  $T_1 = 3 \times 10^{10}$  K, we find that the magnetic field has to be smaller than 3% of the equipartition field to produce the outflow. For the highest temperature  $T_1 = 10^{11}$  K flow, the production of the outflow is possible only when the magnetic field is less than 1% of the equipartition field. So we conclude that the Compton preheated outflow is possible in the magnetic CDAFs as long as the magnetic field is less than from 10% to 1% of the equipartition field.

## 4. Summary and Discussion

Hot accretion flows like ADAFs have a number of physical characteristics that complement the classic low-temperature disk flows. In previous work, we have explored the consequences of the high temperature and the two-dimensional density structure of these flows, and have found that ADAFs may be able to produce radiatively driven outflows. We subsequently have noted that self-similar CDAFs have even more suitable properties for producing outflows as compared to ADAFs: steeper poloidal density gradients and higher radiation efficiencies. In this paper, we have studied the conditions for self-similar two-dimensional CDAFs (NIA; QG) to develop radiatively heated polar outflows.

1. We have found that CDAFs produce enough luminosity and photon energy to drive polar outflows via Compton heating for a reasonable range of mass accretion rate, or, equally, luminosity, as long as the magnetic field is less than from 10% to 1% of the equipartition field. When the electron temperature saturates around  $10^{11}$  K at the inner region, polar outflows

are possible for  $8 \times 10^{-7} \lesssim L/L_E \lesssim 4 \times 10^{-5}$  for radiation efficiency of  $10^{-2}$ , where  $L_E$  is the Eddington luminosity. The luminosity range for which outflow exists is narrower for lower electron temperature flows and disappears completely for electron temperature  $\lesssim 6 \times 10^9$  K

2. In most cases, outflows are well collimated along the rotation axis, with an opening angle typically in the range  $\lesssim 10^\circ$ .

3. If we, instead of taking efficiency as constant, assume that it is proportional to the mass accretion rate  $\dot{m}$ , the solutions are qualitatively the same but are more self similar, i.e., opening angle and outer boundary (in Schwarzschild units) depend less strongly on  $\dot{m}$ .

4. Outflow is more probable for small viscosity parameter  $\alpha$ .

The treatment in this work is not completely satisfactory in the sense that the dynamics and the temperature profiles of CDAFs are not self-consistently solved. However, it was not our intention to solve fully three-dimensional, self-consistent global CDAFs with proper consideration for all gas, radiative, and magnetic processes, which will be eventually needed to fully understand CDAFs. Rather, our goal has been to show that even in the framework of simple self-similar solutions, radiatively heated polar outflows appear as natural consequences of the physical characteristics of CDAFs.

This work is the result of research activities (Astrophysical Research Center for the Structure and Evolution of the Cosmos) supported by Korea Science & Engineering Foundation.

## A. Radiation Field Inside An Optically Thin Spherical Shell

Let's consider an optically thin, uniform radiating shell with radius  $r'$  and the thickness  $\Delta r'$ . The specific intensity at radius  $r$  ( $r < r'$ ) in the direction of  $\vartheta$  (see Figure 7) is given by integration of radiative transfer equation along that direction. If we denote the emissivity (per unit volume per unit solid angle) of the shell as  $\epsilon_\nu/4\pi$ , then the specific intensity is simply the emissivity times the path length,

$$I_\nu = \frac{\epsilon_\nu}{4\pi} \Delta s = \frac{\epsilon_\nu}{4\pi} \frac{\Delta r'}{\cos \phi}, \quad (\text{A1})$$

where  $\phi$  is the angle between the ray and the normal of the shell. From the law of sines,  $\sin \phi = (r/R) \sin \vartheta$ . The radiation energy density,  $E_\nu(r)$ , is given by the integral of  $I_\nu$  over the solid angle  $d\Omega$ ,

$$E_\nu(r) = \frac{1}{c} \int \frac{\epsilon_\nu}{4\pi} \frac{\Delta r'}{\cos \phi} d\Omega \quad (\text{A2})$$

$$= \frac{1}{c} \frac{\epsilon_\nu}{4\pi} \Delta r' \int \frac{\sin \vartheta d\vartheta}{\sqrt{1 - \frac{r^2}{r'^2} \sin^2 \vartheta}} d\varphi \quad (\text{A3})$$

$$= \frac{1}{c} \epsilon_\nu \Delta r' \frac{r'}{r} \ln \sqrt{\frac{r' + r}{r' - r}}. \quad (\text{A4})$$

Equation (A2) formally diverges when  $r \rightarrow r'$  whereas the correct value saturates. In the limit when  $r' - r \lesssim \Delta r'$ , the effect of shell's curvature has to be incorporated in  $\Delta s$ . However, since the radiation energy density is calculated by the sum of contributions from discrete shells in  $r$  (eq. [8]), the divergence is automatically avoided.

## B. Comptonized Synchrotron Emission

The angle-averaged synchrotron emission by relativistic Maxwellian electrons is given by (Pacholczyk 1970)

$$\epsilon_{syn}(\nu) d\nu = \frac{2\pi}{\sqrt{3}} \frac{e^2}{c} \frac{n_e \nu}{\theta_e^2} I'(x_M) d\nu \quad (\text{B1})$$

where  $x_M \equiv 2\nu/(3\nu_0\theta_e^2)$ ,  $\nu_0 \equiv eB/(2\pi m_e c)$ , and

$$I'(x_M) = \frac{4.0505}{x_M^{1/6}} \left( 1 + \frac{0.40}{x_M^{1/4}} + \frac{0.5316}{x_M^{1/2}} \right) \exp(-1.8899x_M^{1/3}) \quad (\text{B2})$$

is a fitting formula (Mahadevan, Narayan, & Yi 1996). When absorption is not important, the cooling rate due to the optically thin synchrotron emission is obtained by integrating the equation (B1)

$$\Lambda_{syn}^0 = 213.6 \frac{e^2}{c} n_e \nu_0^2 \theta_e^2. \quad (\text{B3})$$

However, a large fraction of the low energy synchrotron photons are generally absorbed by synchrotron self-absorption. The synchrotron emission in the presence of absorption can be approximated as

$$\Lambda_{syn} = f_{syn} \Lambda_{syn}^0, \quad (\text{B4})$$

where

$$f_{syn} \equiv \int_{x_M^{abs}}^{\infty} x_M I'(x_M) dx_M / \int_0^{\infty} x_M I'(x_M) dx_M \quad (\text{B5})$$

is the fraction of synchrotron emission above the synchrotron self-absorption frequency  $\nu_{abs}$  which satisfies

$$\tau_{syn} = \frac{1}{4\sqrt{3}} \frac{e^2 c n_e(r) r}{\nu_{abs} k T_e \theta_e^2} I'(\nu_{abs}) = 1. \quad (\text{B6})$$

Thus, we only consider the optically thin part of synchrotron emission as the cooling function for the gas and as a contribution to the preheating radiation field.

Locally emitted synchrotron photons are upscattered by inverse Comptonization off hot electrons. Here, we adopt a simple estimate of Comptonized synchrotron, which is reasonable in physical conditions considered in this paper,

$$\Lambda_{CS} = \eta_{syn} f_{syn} \Lambda_{syn}^0, \quad (B7)$$

where

$$\eta_{syn} = \min(\eta_0, \eta_{syn}^{sat}) \quad (B8)$$

is the Comptonized energy enhancement factor (see e.g., Dermer et al. 1991) for synchrotron emission. The enhancement factor for fully saturated Comptonized synchrotron in the presence of absorption is

$$\eta_{syn}^{sat} = \frac{\int_{x_M^{abs}}^{\infty} \frac{3kT_e}{h\nu} x_M I'(x_M) dx_M}{\int_{x_M^{abs}}^{\infty} x_M I'(x_M) dx_M}, \quad (B9)$$

(see §3.1 for bremsstrahlung case). The synchrotron absorption frequency is compared with that for free-free absorption, and the larger of the two is chosen.

The radiation temperature of locally emitted Comptonized synchrotron is similarly

$$T_X^{CS} = \min(\eta_0 \frac{3}{8} \frac{h\nu_0}{k} \theta_e^2 <x_M>_{\epsilon_\nu}, T_e), \quad (B10)$$

where

$$<x_M>_{\epsilon_\nu} \equiv \frac{\int_{x_M^{abs}}^{\infty} x_M^2 I'(x_M) dx_M}{\int_{x_M^{abs}}^{\infty} x_M I'(x_M) dx_M} \quad (B11)$$

is the energy-weighted mean photon energy in  $x_M$  unit. This treatment of Comptonized synchrotron radiation is almost the same as that adopted in Park & Ostriker (2001), except that the energy enhancement factor and the treatment of saturated Comptonization are slightly improved.

In the presence of both bremsstrahlung and synchrotron emission,  $\Lambda$  is replaced by  $\Lambda_{Cbr} + \Lambda_{CS}$  in equation (8) and  $T_X \Lambda$  by  $T_X^{Cbr} \Lambda_{Cbr} + T_X^{CS} \Lambda_{CS}$  in equation (9).

## REFERENCES

- Abramowicz, M., Chen, X., Kato, S., Lasota, J.-P., & Regev, O. 1995, ApJ, 438, L37  
 Ball, G. H., Narayan, R., & Quataert, E. 2001, ApJ, 552, 221 (BNQ)



- Begelman, M. C., & Meier, D. L. 1982, *ApJ*, 253, 873
- Blandford, R. D., & Begelman, M. C. 1999, *MNRAS*, 303, L1
- Ciotti, L., & Ostriker, J. P. 1997, *ApJ*, 487, L105
- Ciotti, L., & Ostriker, J. P. 2001, *ApJ*, 551, 131
- Cowie, L. L., Ostriker, J. P., and Stark, A. A. 1978, *ApJ*, 226, 1041
- Dermer, C. D., Liang, E. P., & Canfield, E. 1991, *ApJ*, 369, 410
- Ichimaru, S. 1997, *ApJ*, 214, 840
- Igumenshchev, I. V., & Abramowicz, M. A. 1999, *MNRAS*, 303, 309
- Igumenshchev, I. V., & Abramowicz, M. A. 2000, *ApJS*, 130, 463
- Igumenshchev, I. V., Abramowicz, M. A., & Narayan, R. 2000, *ApJ*, 537, L27
- Igumenshchev, I. V., Chen, X., & Abramowicz, M. A. 1996, *MNRAS*, 278, 236
- Levich, E. V. & Syunyaev, R. A. 1971, *Soviet Astronomy*, 15, 363
- Mahadevan, R., Narayan, R., & Yi, I. 1996, *ApJ*, 465, 327
- Narayan, R., Barret, D., & McClintock, J. E. 1997, *ApJ*, 482, 448
- Narayan, R., Igumenshchev, I. V., & Abramowicz, M. A., 2000, *ApJ*, 539, 798 (NIA)
- Narayan, R., Mahadevan, R., & Quataert 1999, in *The Theory of Black Hole Accretion Discs*, eds. M. A. Abramowicz, G. Bjornsson, and J. E. Pringle (Cambridge: Cambridge U. Press), 148 (astro-ph/9803141)
- Narayan, R., & Yi, I. 1994, *ApJ*, 428, L13
- Narayan, R., & Yi, I. 1995a, *ApJ*, 444, 231
- Narayan, R., & Yi, I. 1995b, *ApJ*, 452, 710
- Nobili, L., Turolla, R., & Zampieri, L. 1991, *ApJ*, 383, 250
- Ostriker, J. P., McCray, R., Weaver, R., & Yahil, A. 1976, *ApJ*, 208, L61
- Pacholczyk, A. G. 1970, *Radio Astrophysics* (San Francisco: Freeman)
- Park, M.-G. 1990a, *ApJ*, 354, 64
- Park, M.-G. 1990b, *ApJ*, 354, 83
- Park, M.-G. & Ostriker, J. P. 1999, *ApJ*, 527, 247
- Park, M.-G. & Ostriker, J. P. 2001, *ApJ*, 549, 100
- Quataert, E., & Gruzinov, A. 2000, *ApJ*, 539, 809 (QG)
- Rees, M. J., Begelman, M. C., Blandford, R. D., & Phinney, E. S. 1982, *Nature*, 295, 17

- Shakura, N. I., & Sunyaev, R. A. 1973, A&A, 24, 337
- Stepney, S., & Guilbert, P. W. 1983, MNRAS, 204, 1269
- Stone, J. M., Pringle, J. E., & Begelman, M. C. 1999, MNRAS, 310, 1002
- Svensson, R. 1982, ApJ, 258, 335
- Svensson, R. 1984, MNRAS, 209, 175
- Wandel, A., Yahil, A., & Milgrom, M. 1984, ApJ, 282, 53
- Xu, G., & Chen, X. 1997, ApJ, 489, L29
- Zampieri, L., Miller, J. C., & Turolla, R. 1996, MNRAS, 281, 1183

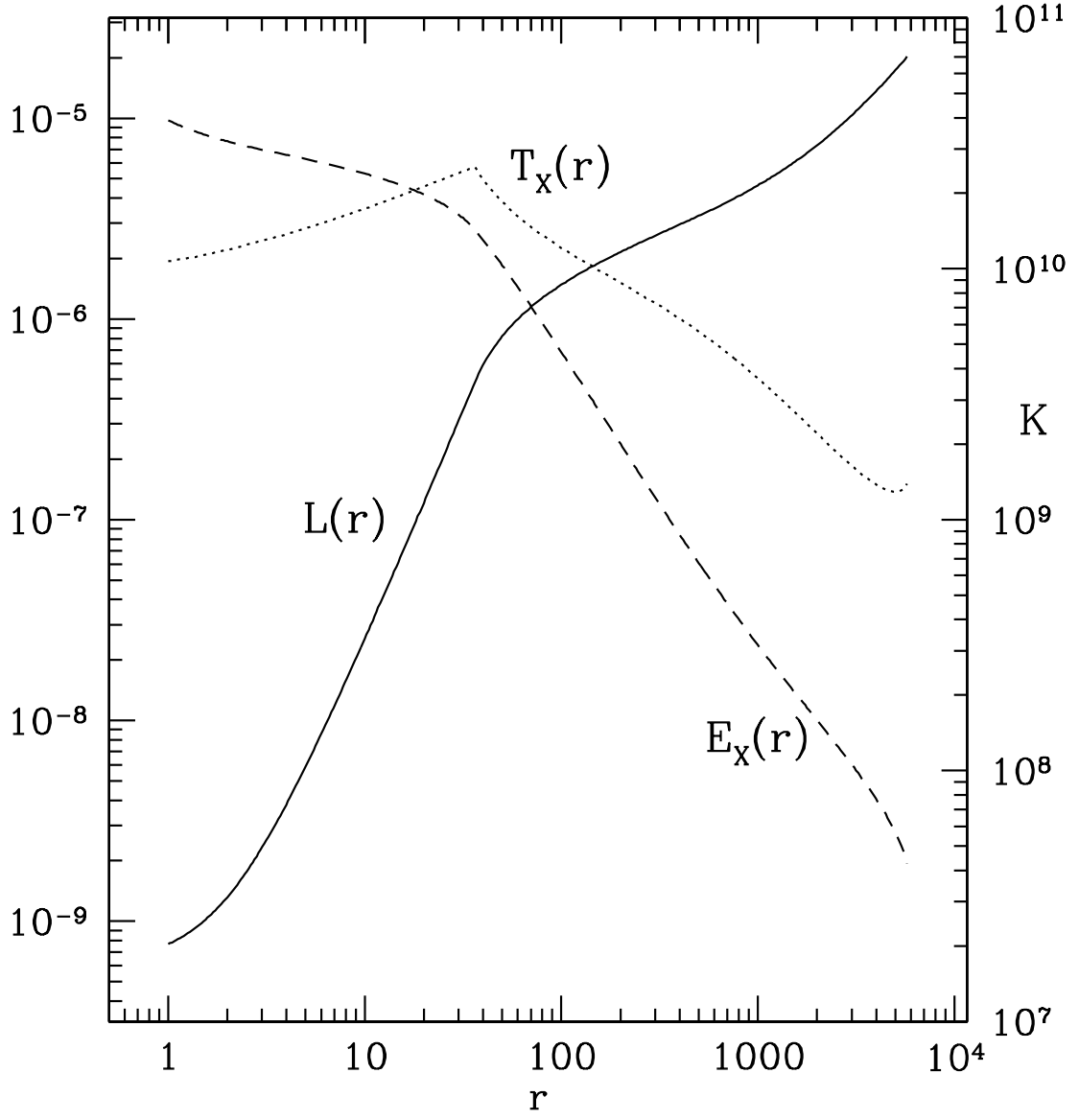


Fig. 1.— Typical log profiles of luminosity  $L(r)$  (in units of  $L_E$ , left ordinate), of the radiation energy density  $E_X(r)$  (in arbitrary units, left ordinate), and of the radiation temperature  $T_X(r)$  (in K, right ordinate).

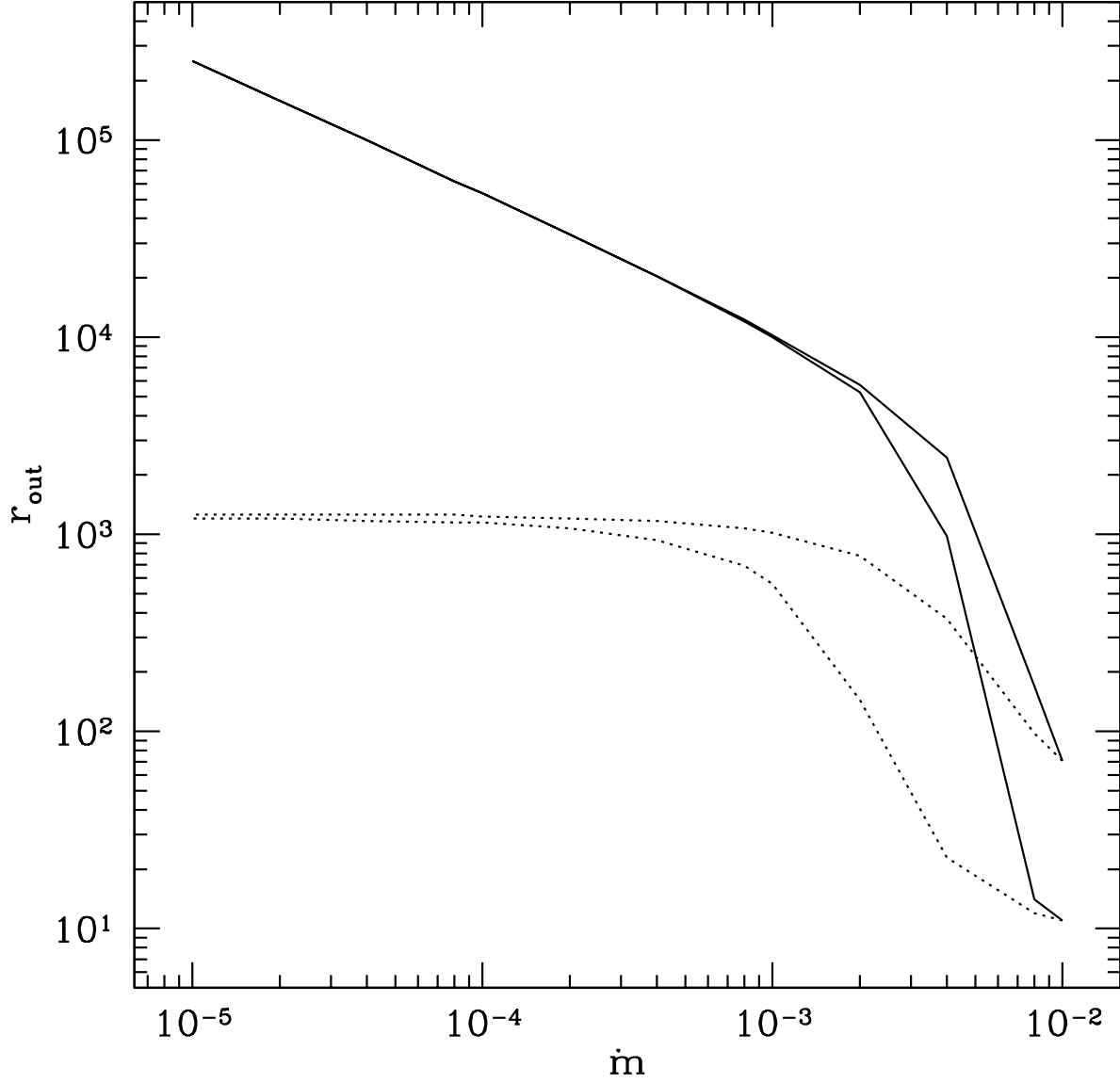


Fig. 2.— The outer boundary radius  $r_{out}$  as a function of  $\dot{m}$ . *Upper solid line* is for  $T_1 = 3 \times 10^{10}$  K and *lower one* for  $T_1 = 10^{11}$  K, both for constant radiation efficiency  $\epsilon_c \eta_c = 0.01$ . *Dotted lines* represent the same  $r_{out}$  for varying radiation efficiency  $\epsilon_c \eta_c = 10^{-2}(\dot{m}/10^{-2})$ : *upper one* for  $T_1 = 3 \times 10^{10}$  K and *lower one* for  $T_1 = 10^{11}$  K.

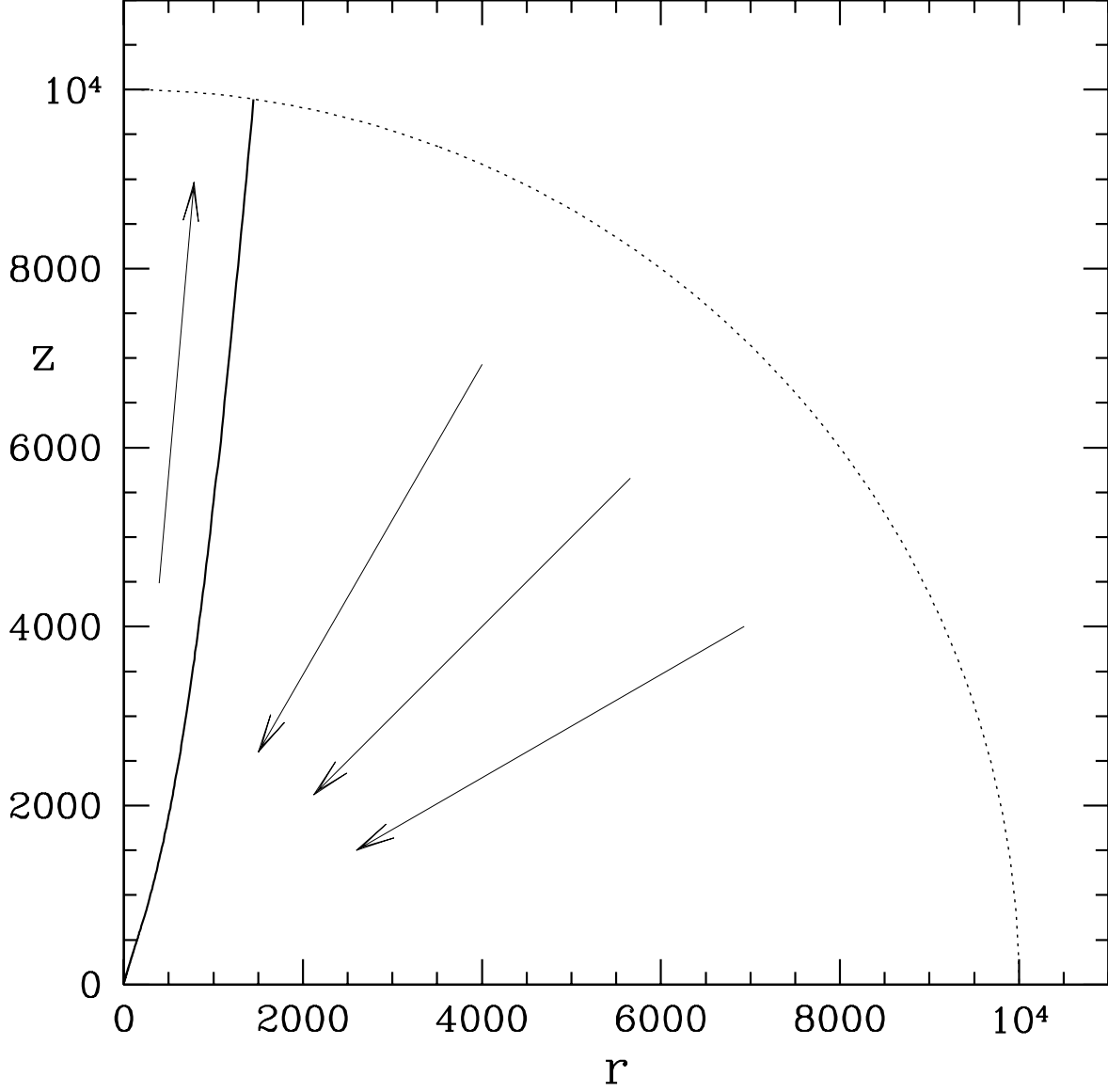


Fig. 3.— The region inside the *solid curve* toward the pole is overheated above the virial temperature due to Compton heating. Outer *dotted circle* shows the outer boundary of CDAF for given total luminosity. This figure is for  $\dot{m} = 10^{-3}$  and  $T_1 = 10^{11}$  K. The opening angle of the outflow at the outer boundary is only  $8^\circ$ .

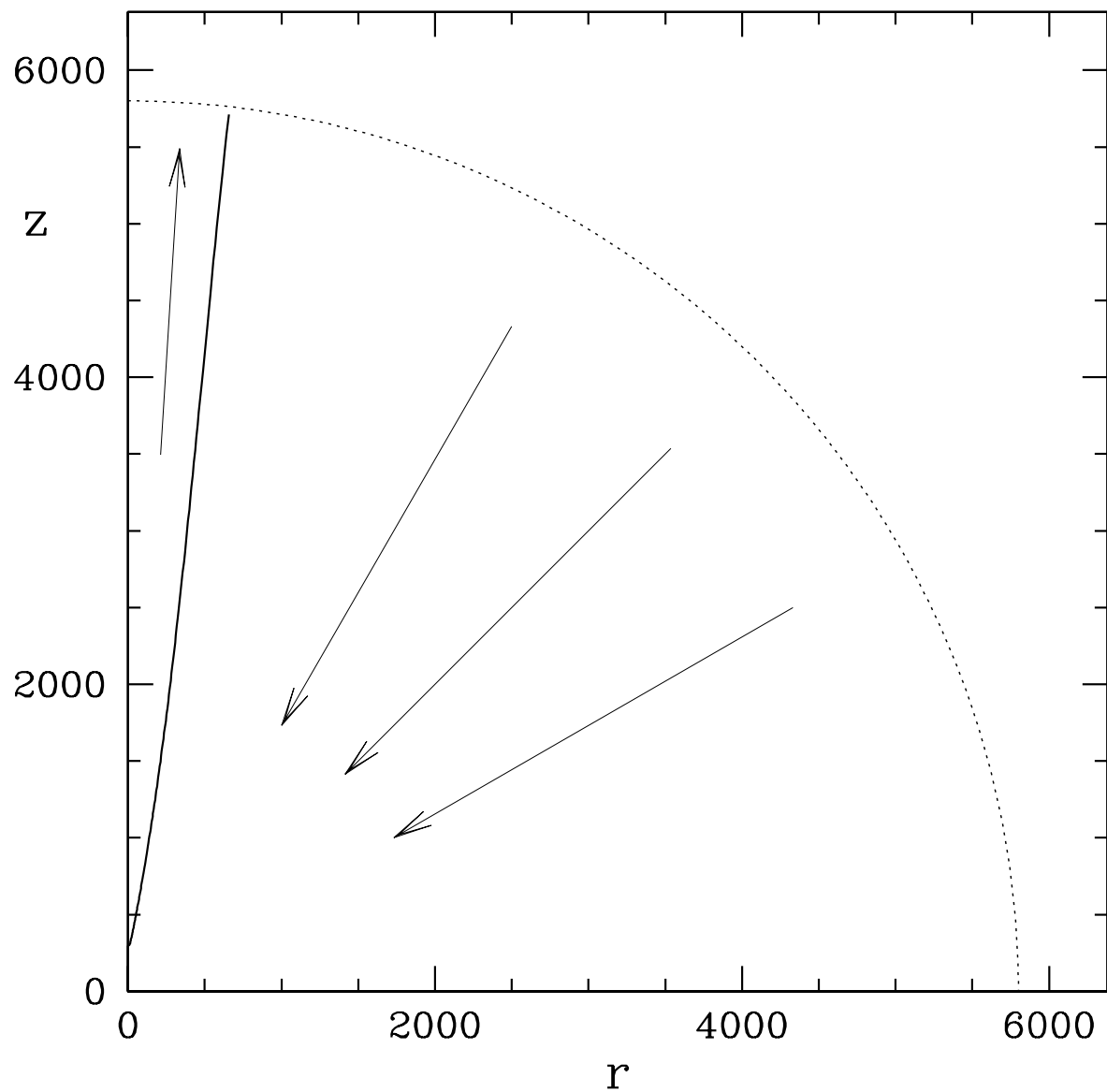


Fig. 4.— Same as Figure 3, but for  $\dot{m} = 2 \times 10^{-3}$  and  $T_1 = 3 \times 10^{10}$  K. The opening angle at the outer boundary is  $8^\circ$ .

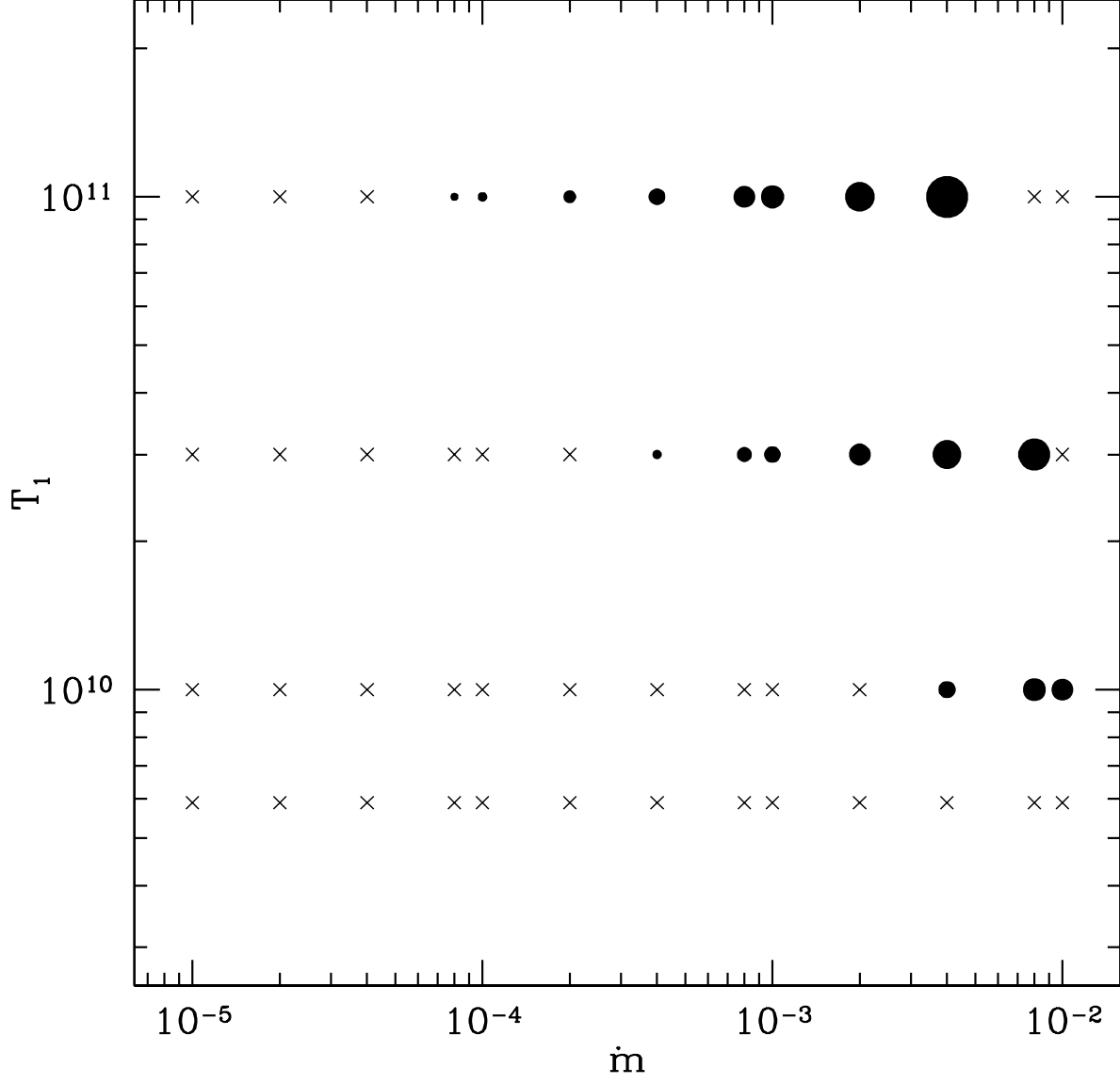


Fig. 5.— The parameter space of  $(\dot{m}, T_1)$  under constant radiation efficiency for which outflow exists is denoted as *circles*. The size of circle represents the opening angle of the outflow at the outer boundary. No outflow is found at  $(\dot{m}, T_1)$  denoted by *crosses*.

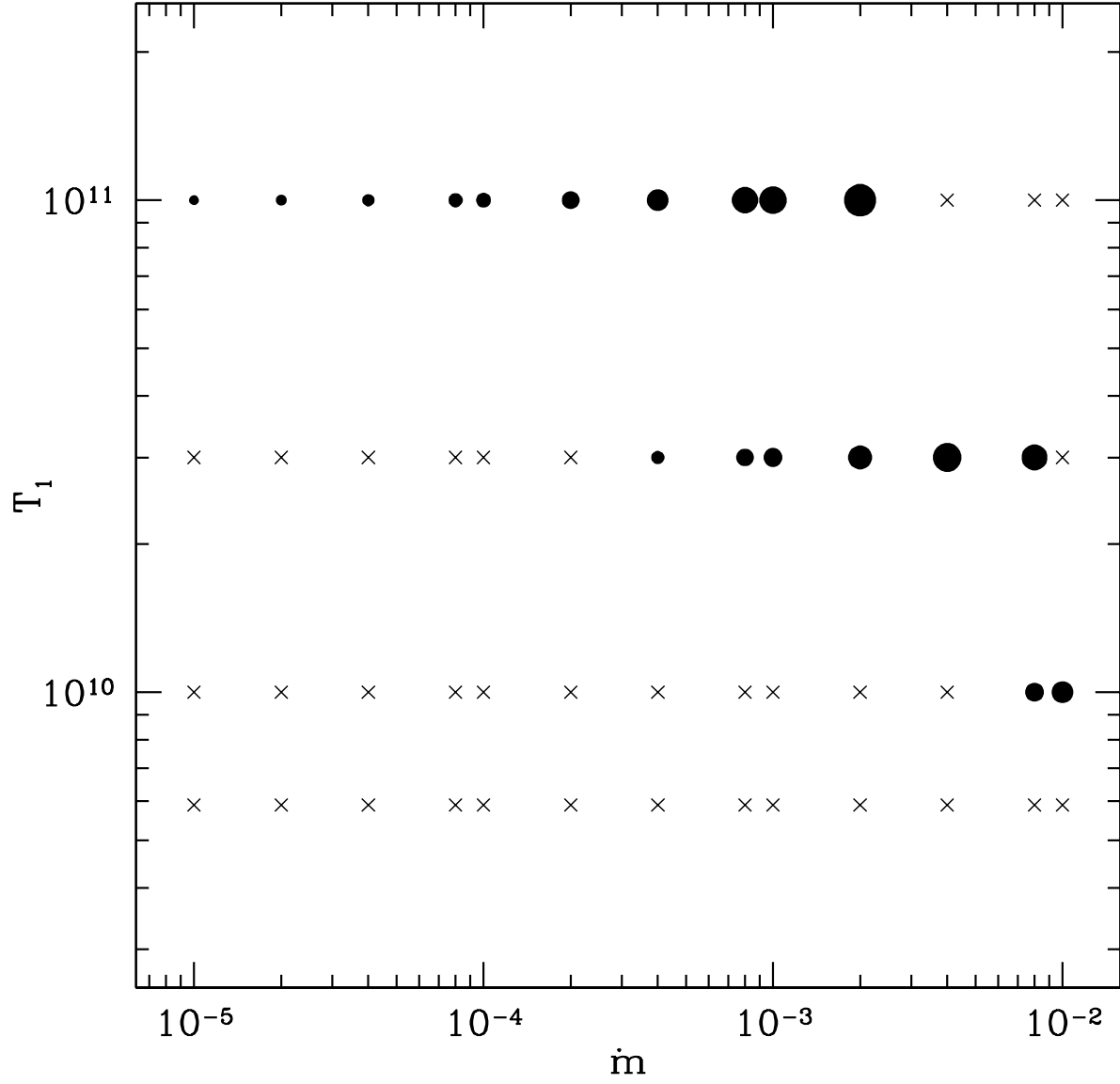


Fig. 6.— Same as Figure 5, but now the radiation efficiency is proportional to the mass accretion rate.



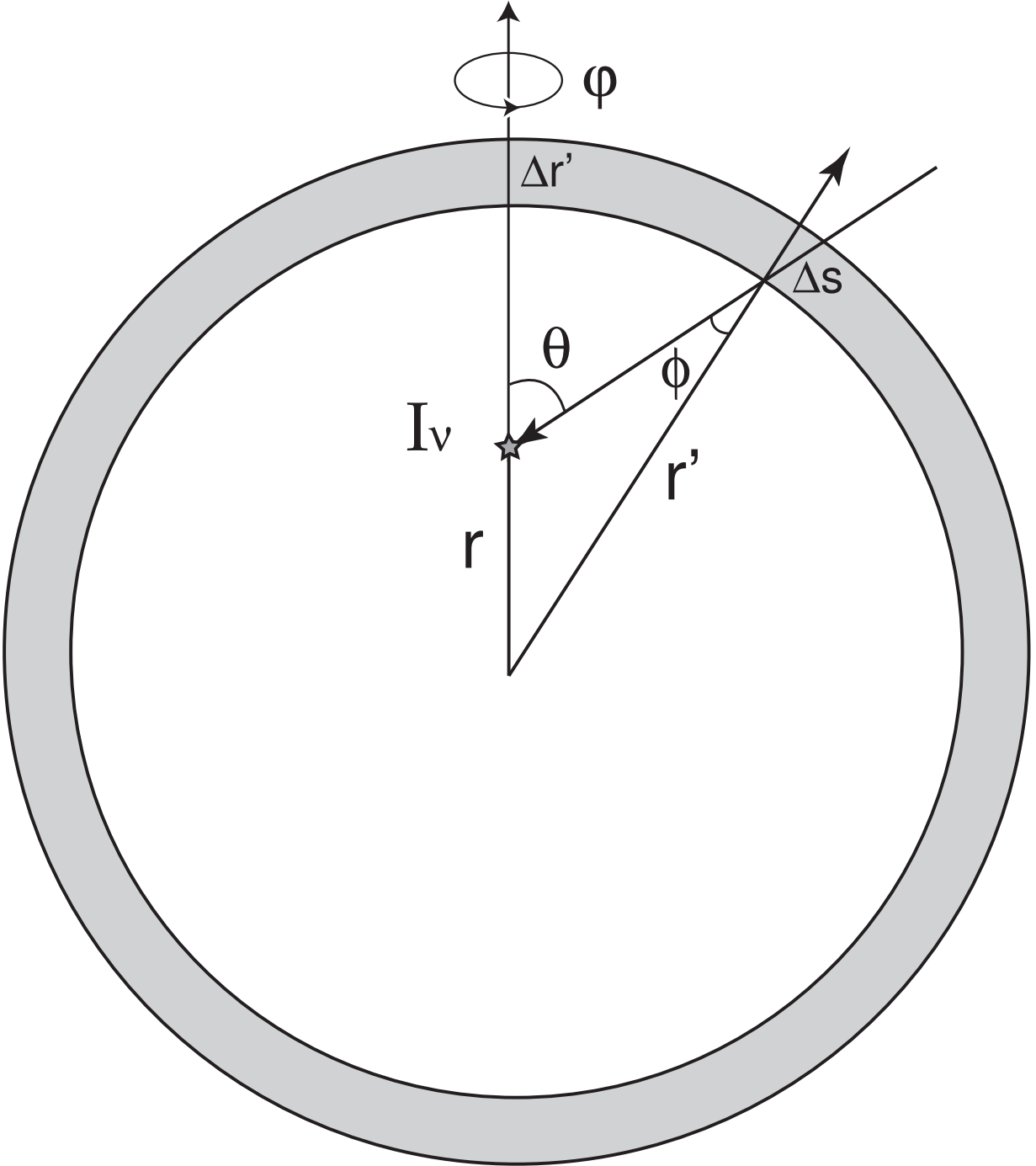


Fig. 7.— The diagram for calculation of specific intensity,  $I_\nu$ , inside a radiating spherical shell.